Calhoun

Institutional Archive of the Naval Postgraduate School

Calhoun: The NPS Institutional Archive

Faculty and Researcher Publications | Faculty and Researcher Publications Collection

2017-02-20

Retrieval of vertical air motion in precipitating clouds using Mie scattering and comparison with in situ measurements

Fang, Ming

American Meteorological Society

Fang, Ming, et al. "Retrieval of Vertical Air Motion in Precipitating Clouds Using Mie

Retrieval of Vertical Air Motion in Precipitating Clouds Using Mie Scattering and Comparison with In Situ Measurements

MING FANG, BRUCE ALBRECHT, AND EUNSIL JUNG[a]

Rosenstiel School of Marine and Atmospheric Science, University of Miami, Miami, Florida

PAVLOS KOLLIAS

School of Marine and Atmospheric Sciences, Stony Brook University, State University of New York, Stony Brook, New York

HAFLIDI JONSSON

Center for Interdisciplinary Remotely-Piloted Aerosol Studies, Marina, California

IVAN POPSTEFANIJA

ProSensing, Inc., Amherst, Massachusetts

ABSTRACT

For the first time, the Mie notch retrieval technique is applied to airborne cloud Doppler radar observations in warm precipitating clouds to retrieve the vertical air velocity profile above the aircraft. The retrieval algorithm prescribed here accounts for two major sources of bias: aircraft motion and horizontal wind. The retrieval methodology is evaluated using the aircraft in situ vertical air velocity measurements. The standard deviations of the residuals for the retrieved and in situ measured data for an 18-s time segment are 0.21 and $0.24 \, \mathrm{m \, s^{-1}}$, respectively; the mean difference between the two is $0.01 \, \mathrm{m \, s^{-1}}$. For the studied cases, the total theoretical uncertainty is less than $0.19 \, \mathrm{m \, s^{-1}}$ and the actual retrieval uncertainty is about $0.1 \, \mathrm{m \, s^{-1}}$. These results demonstrate that the Mie notch technique combined with the bias removal procedure described in this paper can successfully retrieve vertical air velocity from airborne radar observations with low spectral broadening due to Doppler fading, which enables new opportunities in cloud and precipitation research. A separate spectral peak due to returns from the cloud droplets is also observed in the same radar Doppler spectra and is also used to retrieve vertical air motion. The vertical air velocities retrieved using the two different methods agree well with each other, and the correlation coefficient is as high as 0.996, which indicates that the spectral peak due to cloud droplets might provide another way to retrieve vertical air velocity in clouds when the Mie notch is not detected but the cloud droplets' spectral peak is discernable.

1. Introduction

The measurements of vertical air motion in clouds are essential for the study of the dynamic and microphysic processes and their interactions. Aircraft-based sampling offers the advantage of direct (in situ) methods for measuring the vertical air motion and cloud microphysical properties (Nielsen 1992; Stith 1995; Wang et al. 2012; Noh et al. 2013). However, in situ aircraft measurements are limited to 1D (flight level), and aircraft penetrations in areas of strong turbulence can be restricted for safety reasons.

The measurements of vertical air motion in precipitating clouds using Doppler radars have been attempted since the 1960s (Probert-Jones and Harper 1961; Doviak and Zrnić 1993). In the 1980s and 1990s, Bragg scattering (Wakasugi et al. 1986; Gossard 1988; Rogers et al. 1993; May and Rajopadhyaya 1996; Rajopadhyaya et al. 1998) observed by wind profilers (Doppler radars operating at VHF and UHF) was used to extract the vertical air motions. Over the past decade,

[a] Current affiliation: National Institute of Meteorological Sciences, Jeju, South Korea.

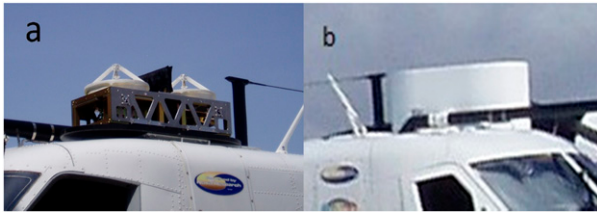*Corresponding author e-mail*: Ming Fang, mfang@rsmas.miami.edu

FIG. 1. The FMCW 95-GHz Doppler radar mounted on the top of the CIRPAS TO research aircraft (a) without and (b) with radome. The radar operates in an upward-looking mode.

the vertical air motion in precipitation has been retrieved using the Mie scattering signatures (Mie 1908) in Doppler spectra, as first proposed by Lhermitte (1988), of short-wavelength (e.g., $\lambda = 3.2$ mm, 95-GHz frequency) cloud radar measurements (Kollias et al. 2002, 2003, 2007; Giangrande et al. 2010). These were measurements from ground-based vertically pointed Doppler radars that can provide a 2D time–height velocity field, but they can only observe the weather phenomena passing over the radar sites.

Airborne Doppler radars enable the study of clouds and precipitation structure over remote locations and oceans (Heymsfield et al. 1996; French et al. 1999; Guimond et al. 2010; Lorsolo et al. 2010; Rogers et al. 2013). Because of their compact design, millimeter wavelength Doppler (cloud) radars operating at 95 GHz are particularly well suited for use on aircraft (e.g., Li et al. 2004; Kollias et al. 2007). The retrieval of the vertical air velocity using Mie scattering signatures on the recorded Doppler spectrum from an airborne 95-GHz Doppler radar has not been performed previously. Here, the Mie technique is applied to the measurements from an airborne cloud Doppler radar during the observations of shallow cumulus over subtropical oceans to retrieve the vertical air velocity profiles in clouds. The retrieval of the vertical air motion is challenged by the aircraft motion that shifts the Mie scattering signatures in the Doppler-velocity space. Moreover, horizontal wind will also contaminate the vertical air velocity retrieval when the radar beam is not vertically pointing. The onboard global positioning system (GPS) provides a high-temporal-resolution attitude determination (angle and velocity) of the aircraft, and the in situ wind measurements can be used to estimate the horizontal wind profile. Using these inputs, the influence of the aircraft motion and horizontal wind on the retrieved vertical air motion can be estimated and removed. The terminal velocity of hydrometers with 1.69-mm diameter can be corrected for air density variations using the aircraft measurements. Subsequently, the vertical air velocities at different heights can be retrieved using the

Mie notch technique and compared with retrievals based on the presence of a cloud Doppler spectral peak. The short-range vertical velocity retrievals are then compared with the in situ aircraft velocity measurements and the retrieval uncertainties are then evaluated.

2. Airborne FMCW cloud Doppler radar

The data used in this study are from the Barbados Aerosol Cloud Experiment (BACEX), which was conducted off the Caribbean Sea from mid-March to mid-April 2010 in Barbados (Jung et al. 2016a), and the Key West Cloud Experiment (KWACEX), which was carried out in May 2012 near Key West, Florida (Jung et al. 2016b). The purpose of BACEX and KWACEX was to observe cloud–aerosol interactions associated with precipitating and nonprecipitating cumuli over the tropical ocean. The principal observing platform for the experiments was the Center for Interdisciplinary Remotely-Piloted Aircraft Studies (CIRPAS) Twin Otter (TO) research aircraft (refer to Fig. 1). During the field experiments, the TO was equipped with instruments that probe aerosol and hydrometeors, measure standard meteorological variables (such as temperature, pressure, and humidity), and observe the mean and turbulent thermodynamic and wind structures. A low-power solid-state frequency-modulated continuous wave (FMCW) 95-GHz (changeable) Doppler radar (Mead et al. 2003) was mounted on the top of the aircraft (normal to fuselage) in an upward-facing mode. The FMCW radar acquires Doppler spectra at a sampling rate (i.e., temporal resolution) of about 3 Hz, with range gates spaced (i.e., range resolution) at 24 m for BACEX and 10 m for KWACEX, and provides users with the fine structures of clouds and precipitations. The fine resolution of FMCW allows radar observation to be proximity to the in situ wind and microphysical measurements. The radar characteristics are summarized in Table 1.

3. Methodology

a. Mie scattering

Light scattering by spheres with size parameters $(x = \pi D/\lambda) \ll 1$ is described by the Rayleigh scattering approximation and the backscattering cross section σ_b (mm^2) is proportional to the sixth power of D, where λ is the wavelength and D is the particle diameter. The monotonic increase of σ_b with particle size is disrupted in the Mie scattering regime ($\sim0.1 < x < 100$), where

TABLE 1. Characteristics of an FMCW radar.

Parameter	Value (Barbados/Key West)
Center frequency (GHz)	94.8/94.1
Wavelength (mm)	3.2
Peak transmit power (dBm)	30
Transmit duty cycle (%)	6.25
PRT (μs)	39.78138/63.145
Chirp pulse bandwidth (MHz)	Variable; up to 20
Max range (m)	5237/3963
Nyquist velocity (m s^{-1})	20/12.6
Range resolution (m)	24/10
Receiver noise figure (dB)	7.0
Antenna diameter (cm)	30 (12 in)
Antenna gain (dB)	49.2
Antenna beamwidth (°)	0.7
FFT No.	512/64
No. of avg	32/55
Radar beam orientation	Up looking (perpendicular to the aircraft centerline)

σ_b displays successive maxima and minima as displayed in Fig. 2. Figure 2a shows the dependency of σ_b, normalized by the raindrop's geometrical cross section, on a raindrop's diameter. The curve in Fig. 2a was obtained from Mie theory (Mie 1908; Lhermitte 2002; Mätzler 2002; Tridon and Battaglia 2015; Tridon et al. 2013) for 95-GHz (3.2 mm) radars by assuming a spherically shaped raindrop. The location of the first Mie minimum or Mie notch is at $D \sim 1.69$ mm. Figure 2b is similar to Fig. 2a, but the raindrop's diameter in Fig. 2a has been replaced by the raindrop's terminal speed. Lhermitte (1988) proposed that, with a unique relationship between the terminal speeds and diameters of drops falling in still air, the first Mie minimum due to σ_b resonances observed in the 95-GHz radar Doppler spectrum can be used to retrieve the vertical air velocity in clouds. More specifically, the vertical air velocity is the difference

between the terminal velocity in still air and the observed fall velocity of the raindrop with 1.69-mm diameter for upward-pointing ground-based radars. For airborne radars, the additional aircraft motion has to be removed. The first Mie minimum at a raindrop diameter of 1.69 mm translates to a raindrop terminal speed of 5.9 m s^{-1} based on the Beard (1985) fit:

$$V_0(\text{cm s}^{-1}) = \exp(5.984 + 0.8515x \\ - 0.1554x^2 - 0.032\,74x^3), \quad (1)$$

where $x = \ln[D\,(\text{mm})]$. This fit (after density correction) provides speeds with a root-mean-square (RMS) deviation from the well-known Gunn and Kinzer (1949) terminal speed data (obtained at 700 hPa, 20°C, and 50% relative humidity) of less than 1% between $D = 0.5$ and 5.8 mm. In fact to obtain Fig. 2b, Eq. (1) has been used. Because the radar-measured Doppler spectrum is the distribution of power among different velocities, Eq. (1) and Fig. 2b can be used to bridge the Doppler spectrum in the velocity domain and Mie theory in the drop size domain. In principle, the first or even the second maximum relating to Mie scattering oscillation can also be used to retrieve the vertical air velocity. However, these features are not as sharply defined as the first minimum, thus the first Mie minimum or the Mie technique is used in this study.

The use of an oblate spheroid model for large raindrops and T-matrix scattering theory (e.g., Mishchenko et al. 1996; Kollias et al. 2002) provides solutions for the maxima and minima of σ_b that differ slightly from those shown in Fig. 2. Nevertheless, the Mie solution due to scattering by spheres is used here since the key research findings of this work are not changed. The associated uncertainty will be discussed in section 7a.
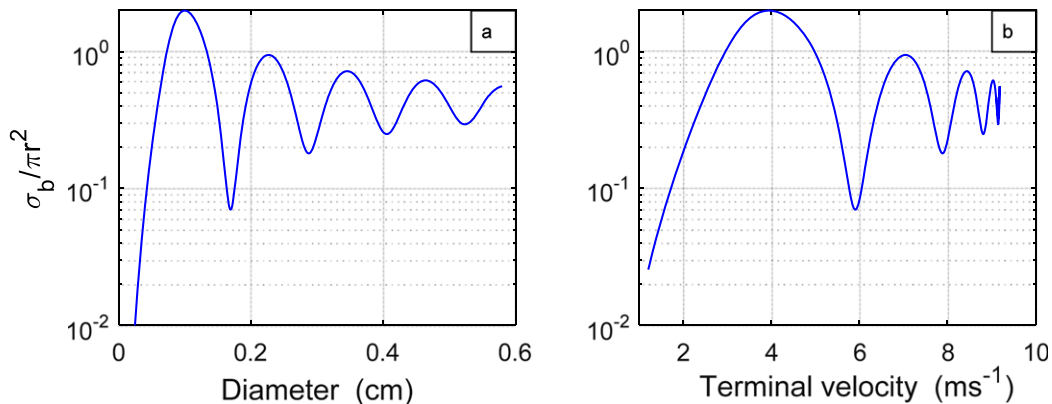

FIG. 2. Dependency of normalized backscattering cross section on the hydrometeor's (a) diameter and (b) terminal speed.
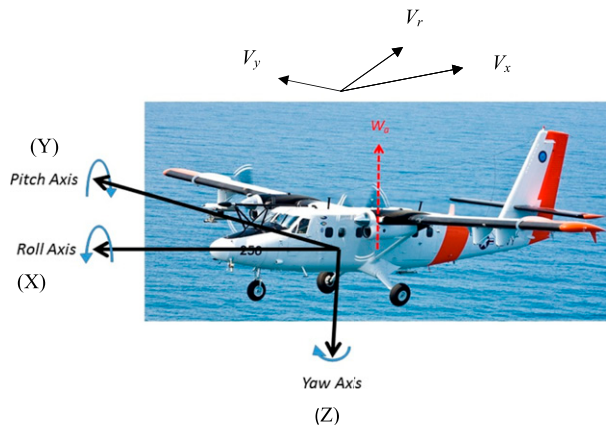
FIG. 3. Relationships among air velocity V_r (relative to aircraft), aircraft vertical velocity W_a, and axes related to aircraft rotations. Three axes form a right-hand-rule coordinate system X–Y–Z, with Z pointing downward.

b. Air-density-corrected terminal speed

Since the terminal speed for a 1.69-mm diameter raindrop obtained using Eq. (1) is the speed at sea level in still air, a density correction is applied to the terminal speed for the observations made aloft at altitude z by using the Beard (1985) formulation,

$$V_f = V_z = \left(\frac{\rho_0}{\rho_z}\right)^m V_0, \qquad (2)$$

where $\rho_0 = 1.194 \, \text{kg m}^{-3}$ is the air density at $z = 0$ for standard conditions. The coefficient m is a function of the raindrop diameter of interest: $m = 0.375 + 0.025D$ (mm). Hereafter, we will designate V_f as a density corrected terminal speed. The V_f in Eq. (2) is V_{f1} (which will be defined later) when V_0 of $D_{1M} = 1.69 \, \text{mm}$ is used, where D_{1M} is the location of the first Mie minimum in terms of particle size. The ρ_z is the air density at altitude z and using the ideal gas law is $\rho_z = p/R_D T_v$ where p is pressure at z and R_D is gas constant for dry air ($287 \, \text{J kg}^{-1} \text{K}^{-1}$). The T_v is the virtual temperature at z and is calculated using $T_v = (1 + 0.608q)T$, where q and T are, respectively, the specific humidity and temperature at z. The speed variation due to density variations with height is about 0.2–$0.3 \, \text{m s}^{-1} \text{km}^{-1}$ for the studied cases.

4. Aircraft motion and equations for its correction

For an airborne upward-pointing Doppler radar, the aircraft motion, horizontal wind, and vertical shear of the horizontal wind can bias the radar-measured Doppler velocity. Figure 3 shows axes associated with possible aircraft rotations and motions. Three axes form a

right-hand rule X–Y–Z coordinate system with Z pointing downward. Since the radar beam is perpendicular to the X–Y plane, if the radar beam is tilted, the radar-observed Doppler velocity will be biased by the projection of the aircraft motion [in the horizontal (V_a) and vertical (W_a)] and the horizontal wind V_h onto the beam axis. The correction in the Doppler velocity due to the aircraft vertical motion is $W_a \cos(P)$ where P is the aircraft pitch angle. In the aircraft reference system, the airspeed V_r is the magnitude of vector $\mathbf{V}_h - \mathbf{V}_a$ or $V_r = \mathbf{V}_h - \mathbf{V}_a$ where $\mathbf{V}_h$ and $\mathbf{V}_a$ are wind and aircraft horizontal velocity vectors relative to the ground. It can be shown that the bias due to V_h and V_a is equal to the projection of V_r onto the radar beam axis. Provided the slip angle (or yaw angle) is $0°$, the V_r is also the aircraft airspeed (the speed of aircraft relative to the air). Furthermore, if the aircraft pitch angle P is $0°$, there will be no bias of the Doppler velocity by V_h and V_a. The TO in level flight has a mean P of about $+3°$ (P positive is nose up); thus, the radar antenna is pointing aft with a positive P, and the Doppler velocity must be corrected by $-V_r \sin(P)$. Thus, for a typical value of $V_r = 60 \, \text{m s}^{-1}$ and $P = 3°$, the correction to the Doppler velocity to obtain the Earth-relative vertical velocity at the level of the aircraft, is about $-3 \, \text{m s}^{-1}$. Fluctuations in the pitch angle due to the turbulent motion of the aircraft also need to be taken into account to correct the Doppler velocity, this is done by using the concurrent measurement of P in the correction of each radar observation.

In addition, the presence of vertical (with distance from the aircraft) shear of V_r due to the vertical shear of the horizontal wind can affect the Doppler velocities when $P \neq 0°$ and/or roll angle $R \neq 0°$. For example, if the airspeed relative to the axis of the aircraft (V_x in Fig. 3) is $10 \, \text{m s}^{-1}$ higher at 1 km above the aircraft, an extra correction due to a $P = 3°$ will be about $0.5 \, \text{m s}^{-1}$. Similarly if V_y, the transverse component of the airspeed (see Fig. 4) is not equal to zero, then variations in R will drive variations in the Doppler velocity equal to $V_y \sin(R)$. It is noteworthy that the air velocity measured at aircraft level cannot be used for other levels because of the vertical shear of horizontal wind speed and direction.

The previous discussions help one to understand how "contaminations" due to aircraft motion and horizontal wind can occur. The real situation could be even more complicated because the aircraft pitch, roll, and slip angles can at the same time be nonzero. Here, the methodology presented by Lee et al. (1994, hereafter L1994) is simplified to remove the contaminations due to aircraft motion and horizontal wind under "complicated"
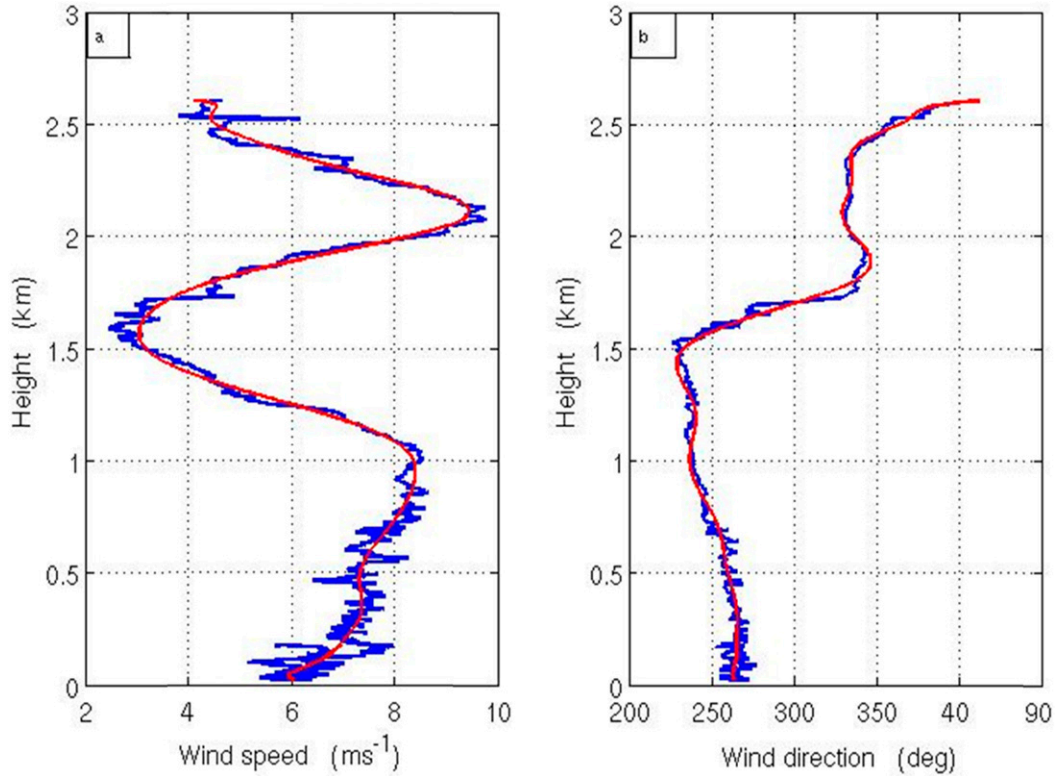
FIG. 4. Vertical profiles of wind (a) speed and (b) direction above sea surface obtained between 1506:00 and 1523:24 UTC 5 Apr 2010 over Barbados. The blue curve represents the measurements, and the red curve is a smoothed profile.

situations. Appendix A provides details on the methodology used. The resultant equations are written as

$$w - v_t = \frac{V_m - I_1 + I_2 - I_3 - I_4}{\sin\phi} + W_a, \tag{3a}$$

$$I_1 = \frac{ux + vy}{r}, \tag{3b}$$

$$I_2 = \frac{V_a(x\sin T + y\cos T)}{r}, \tag{3c}$$

$$I_3 = -\frac{Lx}{r}\left[(1 + \cos P)\cos H\frac{dH}{dt} - \sin P\sin H\frac{dP}{dt}\right], \tag{3d}$$

and

$$I_4 = -\frac{L}{r}\left\{z\cos P\frac{dP}{dt} - y\left[(1 + \cos P)\sin H\frac{dH}{dt}\right.\right.$$
$$\left.\left. + \sin P\cos H\frac{dP}{dt}\right]\right\}, \tag{3e}$$

where V_m is the radar-measured radial velocity; u is the component of the horizontal wind in the east direction; v is the component of the horizontal wind in the north

direction; T is the sum of heading and drift angle; and L is the distance between radar antenna and GPS navigation system, which is about 1 m for our case. Here I_1, I_2, I_3, and I_4 are used to shorten the notation used; the other notations in Eqs. (3) are the same as those in L1994. Relative to Eq. (26) of L1994, I_3 and I_4 have reversed signs because the radar antenna in this study is mounted on the top front of the aircraft, whereas the antenna in L1994 was located on the tail of the aircraft.

On the left-hand side of Eq. (3a), v_t is the mean (terminal velocity) of the spectrum of the particles' terminal velocity distribution and w is the vertical air velocity at a point, which shifts the particle size distribution (PSD) to the left or right by a magnitude of $|w|$. We have here implicitly assumed a uniform vertical air velocity and PSD in a radar resolution volume (Fang et al. 2012; Fang and Doviak 2008).

5. Bias-free Doppler velocity fields

The previous section discusses the bias due to the aircraft motion, horizontal wind, and horizontal wind shear in the radar-measured Doppler spectra. Here,
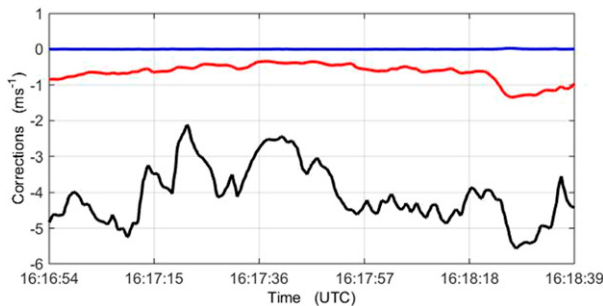
FIG. 5. An example of a time series of correction terms at 228 m ARL related to aircraft motion (black), horizontal wind speed (red), and apparent rotational velocity (blue) for data obtained on 5 Apr 2010 over Barbados.

the procedure used to retrieve a bias-free Doppler velocity is described in detail. In Eq. (3a), V_m is directly measured by the radar and all other terms except I_1 can be determined from the GPS-measured aircraft attitude angles and velocities. The term I_1, or Eq. (3b), represents a contribution from the horizontal wind. To estimate I_1, a seventh-order polynomial fit is performed to the sounding of horizontal wind speed and direction obtained by the aircraft. An example of such fit is shown in Fig. 4, when the TO obtained a sounding from 27 m above the sea level to a height of 2.6-km. The wind speed increased from $6 \, \mathrm{m \, s}^{-1}$ at the sea surface to about $8.5 \, \mathrm{m \, s}^{-1}$ at 1 km and then decreased to $3 \, \mathrm{m \, s}^{-1}$ at 1.6 km; it reached its second maximum of $9.5 \, \mathrm{m \, s}^{-1}$ at 2.1 km before decreasing higher up. The fitted profile of the horizontal wind and the aircraft altitude are used to estimate I_1 at each radar range gate. In Fig. 5, the black curve represents the term $W_a + I_2/\sin\phi$ that is due to aircraft motion (including both horizontal and vertical motion) at 228 m above radar level (ARL); the red curve represents term $I_1/\sin\phi$ due to the horizontal wind and the blue curve represents the term $(I_3 + I_4)/\sin\phi$ that is due to the apparent rotational velocity (L1994). It can be seen that both aircraft motion and horizontal wind terms are significant; aircraft motion is the largest contributor and the contribution from the apparent rotational velocity is negligible. Once all terms are accounted for in the right-hand side of Eq. (3a), the left-hand side of Eq. (3a) can provide us with the mean velocity of a Doppler spectrum without contaminations from the aircraft motion and horizontal wind. By moving the radar-observed original Doppler spectrum a magnitude of $|w - v_t - V_m|$ to the left ($w - v_t - V_m < 0$) or right ($w - v_t - V_m > 0$), one obtains the contamination-removed Doppler spectrum. As has been shown in previous studies (Kollias et al. 2002, 2003, 2007; Giangrande et al. 2010) and will be

subsequently shown here, applying the Mie technique to a contamination-free spectrum, one can find the vertical air velocity w. If w is also removed using Eq. (3), the spectrum of a particle's terminal velocity distribution can be obtained and used to retrieve the PSD.

An example of the zeroth and first moments (Doppler velocity) estimated from the 95-GHz FMCW-recorded Doppler spectra from shallow precipitating cumulus clouds is shown in Fig. 6. The TO penetrated the cloud near the cloud-base level at an airspeed of about $60 \, \mathrm{m \, s}^{-1}$ and an altitude of 768 m above sea level. The TO intercepted several shallow cumulus clouds along this 6-km-long racetrack. Our analysis focused on the shallow convective cloud observed between 1616:46 and 1618:32 UTC in Fig. 6. The average cloud top as observed by the radar was 0.9 km above the aircraft flight level (~1.67 km MSL). Despite its shallow nature, this cloud produced relatively strong radar reflectivity because of the presence of large raindrops located around the dashed line in Fig. 6a. The inspection of the Doppler spectra confirmed the presence of Mie resonance and raindrops with 1.7-mm diameter. Detrained cloud elements into the inversion layer are also seen above 0.9-km level earlier in the penetration 1617:27–1617:37 UTC with tilted features due to the relatively strong wind shear across the inversion layer. Both Figs. 6b and 6c show the Doppler velocity fields. In Fig. 6b, the biases due to aircraft motion and horizontal wind have been removed, whereas in Fig. 6c, they have not. In comparing Figs. 6b and 6c, one can see that the predominant upward motion in clouds before the bias is removed has been replaced by predominant downward motion after the bias is removed. The corrected Doppler velocity (Fig. 6b) shows downward motion mostly associated with the precipitation shaft. However, alternating up- and downward motions inside the cloud are noticeable, which implies the possibility of some recirculation within the cloud that may help the growth of larger droplets. But interpretation of the mean Doppler velocities is not straightforward because of the presence of the embedded vertical air motion in the presence of precipitation. Newly growing clouds without precipitation are also shown in Fig. 6 (echoes at around 1616:56, 1617:12, and 1617:20 UTC) and exhibit relatively weak returns with strong updrafts. Figure 7 shows another case for the data obtained on 22 May 2012 in Key West. Again, the predominant upward motion in clouds before the aircraft motion and horizontal wind bias is removed has been replaced by predominant downward motion after the bias is removed. A tilted high-reflectivity core indicates a relatively strong shear layer about 1 km above radar antenna. The vertical dashed lines in Fig. 7 indicate a 20-s time period during which the Mie
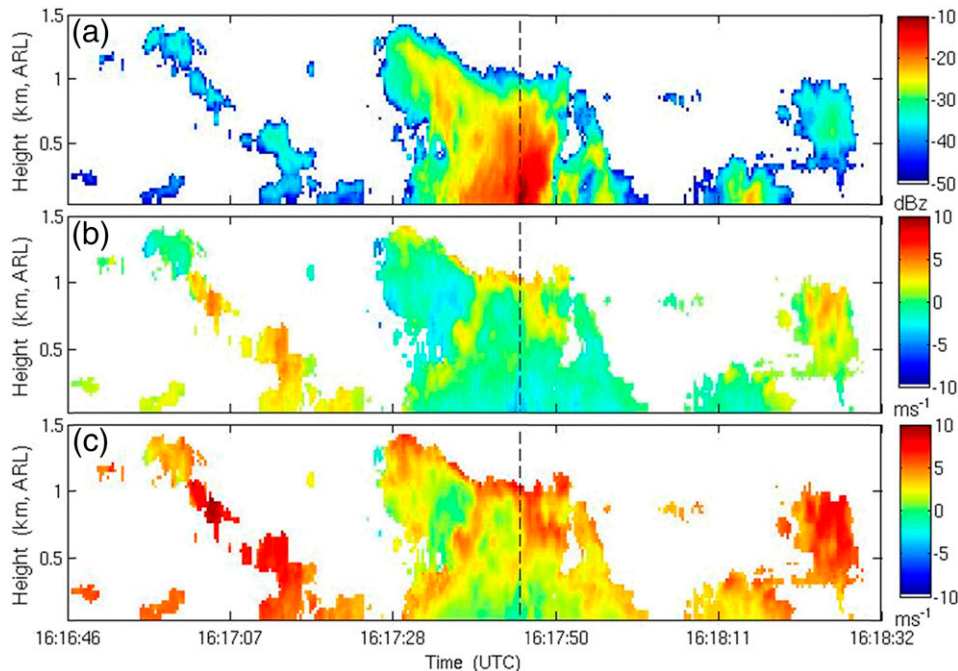
FIG. 6. Time–height cross section of (a) radar reflectivity, (b) bias-removed Doppler velocity (+ upward), and (c) bias-unremoved Doppler velocity in a precipitating cloud on 5 Apr 2010 during BACEX from 1616 to 1618 UTC. The reported height is ARL. Zero height corresponds to 768 m MSL. The dashed line indicates the specific time for the Doppler spectra in Fig. 8.

notches are observed and the radar-retrieved vertical air velocities will be compared with the in situ measurements and will be discussed in section 7. The half transparent regions between two dashed lines result from two images being overlapped and show the regions in which a Mie notch is not recognized. Close inspection reveals two possible reasons for this unrecognizability. One is that the Doppler spectrum is narrow and the Mie notch is beyond its coverage. Another is that the Mie notch is invisible or not detectable in a sufficiently broad Doppler spectrum appearing in a region with relatively strong turbulence. Turbulence is ubiquitous in clouds. The spectrum due to relatively strong turbulence can convolve with the PSD in such a way that Mie notch is smeared out and not discernable or detectable, which is the main reason for the most observations in the transparent regions in Fig. 7. For the Barbados case, the time period for Mie notch being observed is about 5 s.

6. Retrieval of vertical air velocity profile

First, the observed radar Doppler spectra are shifted in velocity space to correct for the aircraft motion and horizontal wind. Subsequently, the airborne radar-observed Doppler spectra can be used to retrieve vertical air velocity (Lhermitte 1988; Kollias et al. 2002;

Giangrande et al. 2010) when the Mie minima can be identified. Figure 8 shows Doppler spectra, smoothed using a third-order Savitzky–Golay filter (Savitzky and Golay 1964; Schafer 2011), at a single range gate observed by the FMCW cloud radar at 1617:44 UTC (indicated by the dashed line in Fig. 6) on 5 April 2010 in Barbados. Negative Doppler velocities indicate motions toward the radar (downward); thus, the largest precipitation particles in the radar sampling volume are on the left side of the Doppler spectra. The blue curve represents the original spectra, whereas the black curve represents spectra with bias removed. Noticeably, there are three spectral peaks. The two spectral peaks on the left are caused by relatively larger raindrops and Mie scattering oscillations; the peak on the right is from relatively smaller cloud droplets whose interaction with the 95-GHz electromagnetic radiation is described by Rayleigh scattering. These smaller hydrometeors are very good tracers of the vertical air motion because of their negligible fall velocity (Kollias et al. 2001). We believe this is the first time that two different signatures of vertical air motion (Mie resonant scattering from raindrops and Rayleigh scattering from cloud droplets) have been simultaneously observed in the same radar Doppler spectrum. The time period of the cloud spectral peak being observed is about 9 s for the Barbados case
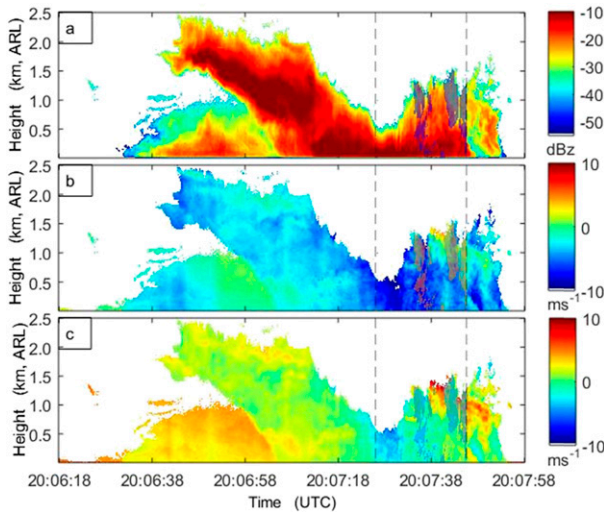
FIG. 7. As in Fig. 7, but for 22 May 2012 over Key West. Zero height corresponds to 500 m MSL. The dashed lines indicate a time period during which radar-retrieved vertical air velocity and in situ measurements will be compared in section 6.
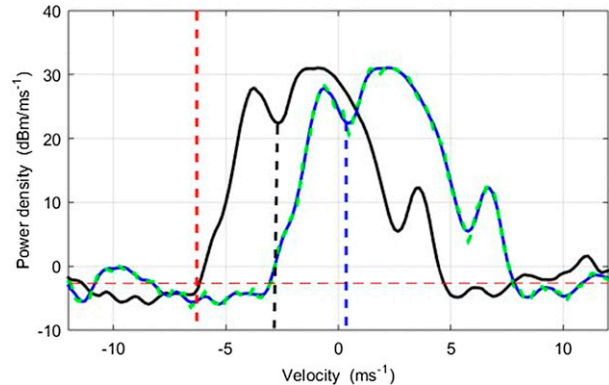

FIG. 8. Original spectrum with bias (green), smoothed spectrum with bias (blue), and smoothed spectrum without bias (black), observed at 252 m ARL at 1617:44 UTC 5 Apr 2010 over Barbados. The various lines are V_{fl} (vertical red dashed line), Mie notch location with bias (blue dashed line), Mie notch location without bias (black dashed line), and the noise level (horizontal red dashed line).

and no cloud spectral peak is observed for Key West case. In Fig. 8, the vertical red dashed line indicates the theoretical terminal velocity of a raindrop with $D = 1.69$ mm in absence of aircraft and air motion, that is $-V_{fl}$, which is $-6.23 \, \mathrm{m \, s^{-1}}$ and has been corrected to the height where the spectrum is obtained. The blue dashed line at $0.31 \, \mathrm{m \, s^{-1}}$ indicates the location of the first Mie minimum of the original spectrum in which the biases have not been removed. The black dashed line at $-2.66 \, \mathrm{m \, s^{-1}}$ indicates the location of the first Mie minimum on the bias-removed spectrum. Relative to the original spectrum, it has been shifted about $3 \, \mathrm{m \, s^{-1}}$ to the left. Considering Eq. (3a) and the assumptions of uniform vertical air velocity and PSD in the radar resolution volume, it is easy to see that the vertical air velocity is the difference between black and red dashed lines, that is $3.57 \, \mathrm{m \, s^{-1}}$. Figure 9 shows another case for the data obtained at 105 m above radar around 2007:28 UTC (indicated by the left dashed line in Fig. 7) on 22 May 2012 in Key West where only two peaks due to Mie scattering are observed. Differently from that in Fig. 8, the Mie notch in the bias-removed spectrum is located on the left of the red dashed line, which implies an approximate $1.6 \, \mathrm{m \, s^{-1}}$ downward vertical air motion.

This procedure for retrieving vertical air velocity at a single radar range gate can be easily extended and applied to all range gates to obtain the vertical velocity profile. Figure 10 shows a bias-removed Doppler spectrogram observed by the FMCW airborne cloud radar at 1617:45 UTC 5 April 2010 over Barbados. Also shown in Fig. 10 are the profiles of the

Mie maxima, Mie notch, vertical air velocity retrieved from Mie notch, and the cloud droplet peak (or vertical air velocity retrieved from cloud droplet peak). Such a clear separation of the spectral maxima associated with the Rayleigh scattering from the cloud droplets and the maxima and minima due to Mie scattering from raindrops in the same W-band radar Doppler spectrogram, has not been documented previously. The Mie maxima at 36 m above radar (denoted by black and green circles in Fig. 10) are separated by approximately $3 \, \mathrm{m \, s^{-1}}$ (centers at around -3 and $-6 \, \mathrm{m \, s^{-1}}$)—a difference that is equal to the value predicted by Mie theory as shown in Fig. 2b. The blue circles in Fig. 10 represent spectral peaks from the cloud droplets' return; they also indicate the vertical air velocities at different heights because of their negligible terminal speeds
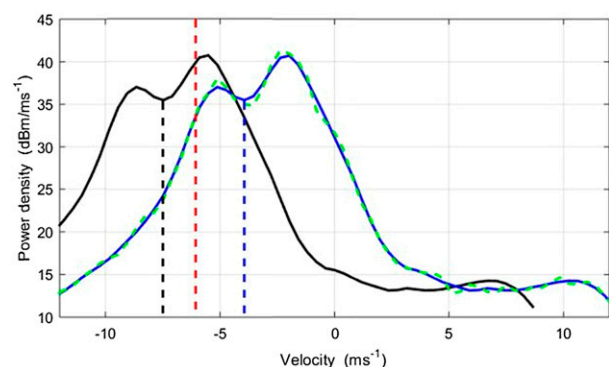

FIG. 9. As in Fig. 8, but for the data observed at 105 m ARL at 2007:26 UTC 22 May 2012 over Key West. The noise level is ~ -4.2 dBm and is not shown.
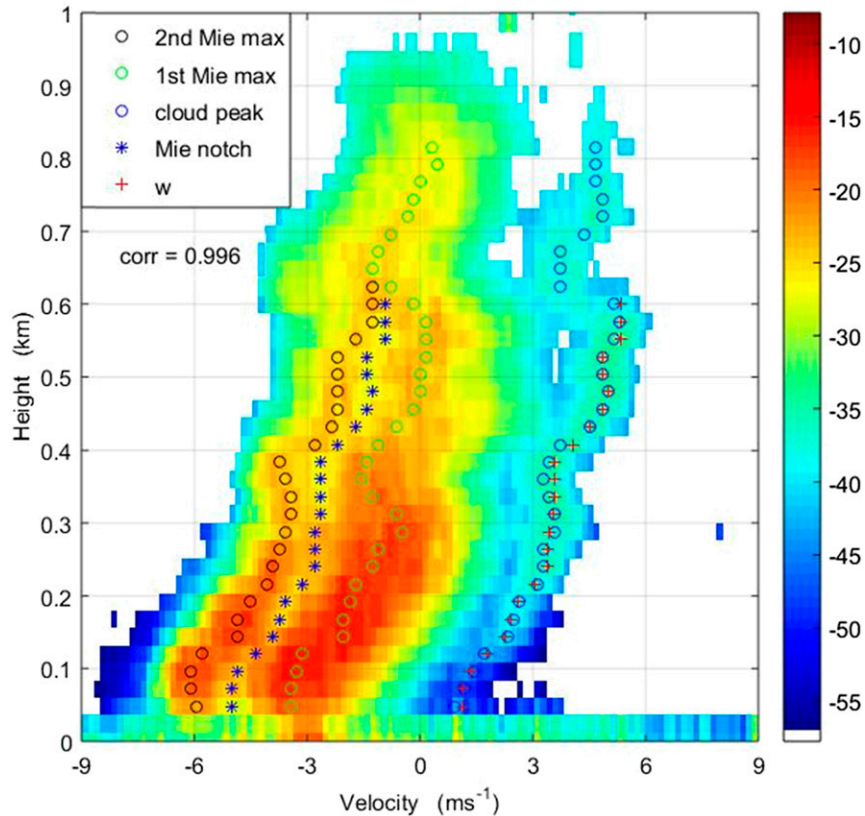
FIG. 10. Bias-free Doppler spectrogram and vertical profiles of the first Mie maximum (green circle), second Mie maximum (black circle), cloud droplet peak or vertical air velocity from cloud droplet peak (blue circle), Mie notch (blue asterisk), and retrieved vertical air velocity from Mie notch (red + sign). Data were obtained at 1617:45 UTC 5 Apr 2010, which is denoted as the vertical dashed line in Fig. 6.

(e.g., $0.3\,\mathrm{cm\,s}^{-1}$ for $D = 10\,\mu\mathrm{m}$). The blue star asterisks indicate the locations of the first Mie minima. Vertical air motion, as a function of height, retrieved using the Mie technique is shown as a red cross. It can be seen that the vertical air motion obtained from cloud droplets agrees well with those retrieved from the Mie technique. The magnitude of an updraft in this cumulus cloud increases with height from $\sim 1\,\mathrm{m\,s}^{-1}$ at 36 m to $\sim 5\,\mathrm{m\,s}^{-1}$ at about 600 m above the radar. The mean difference between the vertical air velocities obtained from the Mie technique and the cloud droplets is $0.05\,\mathrm{m\,s}^{-1}$, with a standard deviation of $0.13\,\mathrm{m\,s}^{-1}$, and the correlation coefficient between them is 0.996. This very high correlation implies that the well-defined cloud droplet spectral peak can be also used to retrieve vertical air velocity when Mie notch technique is not applicable. However, any uncertainties due to aircraft motion corrections can also affect both the Mie technique and the direct cloud droplets' retrievals. Furthermore, air velocities retrieved from the Mie technique require a density correction to the terminal speed of the 1.69-mm droplets; while no

density correction is needed for the air motion retrieved directly from the cloud droplets. Uncertainties in vertical air velocity retrieval will be discussed in detail in the next section.

Figure 11 shows a time–height cross section of the retrieved vertical air velocity during the time period indicated by the dashed lines in Fig. 7. The white void areas are primarily due to the Mie notch being unrecognizable or nonexistent. It can be seen that downward motion prevailed during the first 4 s in the cloud. In the second 4 s, downward and upward motions alternately existed. The strongest updrafts appear in the next 6 s, which may indicate a growing new cell. Although upward motion prevailed in the last 6 s in most areas, strong downward motion appeared around 2007:43 UTC from the cloud base up to about 200 m above the radar. Those observed features of the vertical air velocity more directly relate to the cloud dynamics and microphysics and are different from that shown in Fig. 7b where the particles' terminal velocities and vertical air velocities had not been separated.
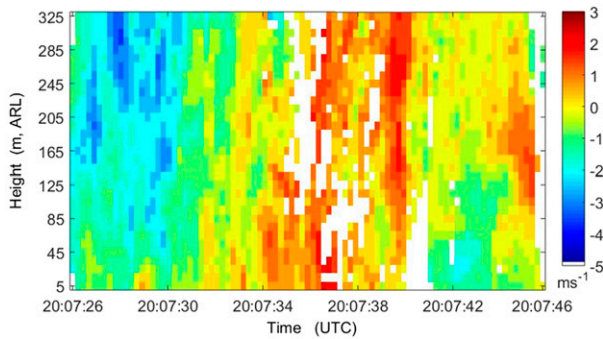
FIG. 11. Time–height cross section of retrieved vertical air velocity for data observed on 22 May 2012 over Key West. White areas primarily result from unrecognizable Mie notch signature or no Mie notch at all.

7. Uncertainties and comparisons of retrieved velocities with in situ measurements

Up to this point, the methodology for retrieving the vertical air velocity from the airborne FMCW cloud Doppler radar observations has been introduced. This section will discuss uncertainties associated with the retrieval procedure and compare the retrieved velocities with in situ measurements.

a. Uncertainties

1) UNCERTAINTY DUE TO AIRCRAFT ATTITUDE ANGLES AND VELOCITY

Heymsfield (1989) discussed bias and uncertainties in airborne radar-measured radial velocities. Both aircraft motion and the horizontal wind can cause bias, but the uncertainties are primarily due to aircraft motion terms. Since Eqs. (3) are used, if both emitting and receiving antenna beams are perfectly perpendicular to the X–Y plane, the bias due to aircraft motion and horizontal wind will be removed. However, radar beams may not be perfectly perpendicular to the X–Y plane because of imperfect installation or vibration caused by air dynamics during a flight or some unknown reasons. Furthermore, the uncertainties can still exist because of the uncertainties in aircraft horizontal and vertical velocities as well as the aircraft attitude angles. The uncertainty associated with radar beam pointing angle will be discussed in next section. The uncertainty of TO attitude angles is less than 0.1° and the uncertainty of aircraft vertical velocity is $0.05\,\mathrm{m\,s^{-1}}$ (Kalogiros and Wang 2002), which is much better than $0.5\,\mathrm{m\,s^{-1}}$ given by Heymsfield (1989) for his case. Although the uncertainty of aircraft horizontal velocity given by Kalogiros and Wang (2002) is $0.02\,\mathrm{m\,s^{-1}}$, $0.05\,\mathrm{m\,s^{-1}}$ will be used here as a conservative estimate. Considering

uncertainty as a random variable and ±0.05 as 1 standard deviation from its mean, the variance associated with horizontal velocity is $(0.05)^2$. The uncertainty related to aircraft vertical motion is equal to the uncertainty of the aircraft vertical velocity itself, which is $0.05\,\mathrm{m\,s^{-1}}$ for a TO (Kalogiros and Wang 2002) and the associated variance is also $(0.05)^2$. Assuming the processes related to the two uncertainties are independent from each other, the total variance is $(0.05)^2 + (0.05)^2$ and the standard deviation or the total uncertainty is approximately equal to $0.07\,\mathrm{m\,s^{-1}}$ (Papoulis and Pallai 2004).

2) BIAS AND UNCERTAINTY OF RADAR BEAM POINTING ANGLE

Previous discussions about bias removal implicitly assume that the radar antennas emitting and receiving electromagnetic waves are exactly aligned along the X axis and the radar beam is exactly perpendicular to the X–Y plane in aircraft coordinates. However, these assumptions may not necessarily be valid. Furthermore, even if these assumptions are true in still air, they may not be valid because of air dynamics or aircraft vibrations. Bias and errors associated with antenna aliment and radar beam pointing angle also can lead to additional bias and uncertainty of the Doppler velocity estimate, and those in turn can lead to the bias and uncertainty of the vertical air velocity retrieval. Calibrating the radar beam pointing angle as done by Haimov and Rodi (2013) might be the best way to account for this bias and uncertainty, but this is beyond the scope of our study. Although the bias and uncertainty of the beam pointing angle are not clear, they should be small and insignificant based on the comparison given in section 7b. By using a high-accuracy inertial geopositioning system and the radar observations of the Earth surface, Haimov and Rodi (2013) found that the RMS error of the radar beam pointing angle is less than 0.03° and the Doppler velocity estimate error is less than $0.05\,\mathrm{m\,s^{-1}}$ for their airborne Wyoming Cloud Radar. This value will be used to calculate the total theoretical uncertainty. The reasonability of this usage will be further justified in the section 7b.

3) UNCERTAINTY DUE TO INACCURATE POSITIONING OF THE MIE NOTCH

In contamination-removed Doppler spectra, the first Mie minimum or Mie notch is used to determine the fall velocity of a cloud droplet with a 1.69-mm diameter. Thus, the inaccurate positioning of the Mie notch in a Doppler spectrum will lead to an error in the retrieved vertical air velocity. By employing simulation, Lhermitte (2002) found that the standard deviation was

$0.066\,\mathrm{m\,s^{-1}}$ in determining the first Mie minimum location from a third-order-polynomial-fitted Doppler spectrum. This value should be applicable to our study too, since we determined the first Mie minimum locations from the Doppler spectra that have been smoothed using a third-order Savitzky–Golay filter (Savitzky and Golay 1964; Schafer 2011).

4) UNCERTAINTY DUE TO QUANTIZATION AND NONSPHEROIDAL SHAPE OF RAINDROPS

Doppler spectra are generated from discrete velocities with a resolution of $0.1563\,\mathrm{m\,s^{-1}}$ for Barbados data and $0.3938\,\mathrm{m\,s^{-1}}$ for Key West data, and therefore there is an associated quantization uncertainty. Based on the theory of statistical signal processing, assuming quantization noise is uniform and white, the standard deviation of the noise can be calculated as $\sqrt{\Delta^2/12}$, where Δ is the quantization step (Papoulis and Pallai 2004). For our case, Δ is the velocity resolution, and the associated quantization uncertainties for BACEX and KWACEX are $\sqrt{0.1563^2/12} \approx 0.045\,\mathrm{m\,s^{-1}}$ and $\sqrt{0.3938^2/12} \approx 0.114\,\mathrm{m\,s^{-1}}$, respectively.

To use Mie theory, we have assumed that small raindrops are spherical in shape. If the raindrops are oblate spheroids, one can use the T-matrix method to determine the first Mie minimum location, which is at about $1.71\,\mathrm{mm}$ (Kollias et al. 2002), and this adds another $0.046\,\mathrm{m\,s^{-1}}$ to the uncertainty.

5) UNCERTAINTY DUE TO DOPPLER FADING

In certain cases, the radar Doppler spectrum can be broadened (Doppler fading) by the projection of scattering particle motion perpendicular to the line of sight (Sloss and Atlas 1968; Kollias et al. 2014). The spread of the projection depends on the magnitude of the motion of the scatterers in the transverse direction and the antenna beamwidth. For circular antenna patterns, the additional broadening $\sigma_D \approx 0.3 V_A \theta_{3\mathrm{dB}}$ where V_A is the aircraft speed ($60\,\mathrm{m\,s^{-1}}$ for TO) and $\theta_{3\mathrm{dB}}$ is the 3-dB beamwidth of the antenna in radians. For our case, the estimated broadening due to Doppler fading is $0.22\,\mathrm{m\,s^{-1}}$ and the related uncertainty is less than $0.1\,\mathrm{m\,s^{-1}}$. The impact of this additional broadening on our ability to detect the Mie notch in the radar Doppler spectra and the introduced uncertainty in estimating the location of the Mie notch is discussed in appendix B.

6) BIAS DUE TO NONUNIFORM BEAMFILLING

The nonuniform distribution of the radar reflectivity field within the radar resolution volume in combination with the use of a high-speed platform can cause biases in the estimation of the Doppler velocity (Tanelli et al. 2002; Sy et al. 2014). Assuming that the reflectivity field varies linearly along the transverse direction within the radar resolution volume, the Doppler velocity bias introduced by nonuniform beamfilling (NUBF) is given by [Eq. (17) in Sy et al. (2014)]

$$\alpha_{\mathrm{linear}} = \frac{V_a}{h_{\mathrm{range}}} \frac{\ln 10}{40 \ln 2} r_{\mathrm{transverse}}^2,$$

where a typical range of $1\,\mathrm{km}$ from the aircraft is used ($h_{\mathrm{range}} = 1\,\mathrm{km}$) and the radius of the footprint of the FMCW radar is $r_{\mathrm{transverse}} = 0.2\,\mathrm{m}$. The estimated coefficient is $\alpha_{\mathrm{linear}} = 0.0066\,\mathrm{m\,s^{-1}\,dBZ^{-1}\,km}$. Thus, a moderate linear gradient of $5\,\mathrm{dBZ\,km^{-1}}$ will cause a Doppler velocity bias of $0.033\,\mathrm{m\,s^{-1}}$. This is comparable to the spectral velocity resolution and, considering that its sign will change as the radar beam moves from positive to negative transverse gradients of the reflectivity, should be neglected for most cases. In any case, the radar reflectivity field measured by the 94-GHz FMCW radar can be used to estimate the radar reflectivity gradient and subsequently provide an indicator of areas where an NUBF correction may need to be considered.

7) TOTAL UNCERTAINTY

Previous sections discussed various contributors to the vertical air velocity retrieval uncertainty. Assuming these uncertainties are due to random variability, the processes associated with them are independent from each other and each uncertainty is a standard deviation from its mean, then the total variance will be the sum of the square of each uncertainty (Papoulis and Pallai 2004). The square root of the total variance is $0.16\,\mathrm{m\,s^{-1}}$ for the Barbados data and $0.19\,\mathrm{m\,s^{-1}}$ for Key West data; these are the total standard deviations or the magnitudes of the total uncertainties.

b. Comparison of retrieved velocities with in situ measurements

The Mie notch technique has been used to retrieve vertical air velocity for more than two decades since Lhermitte proposed it in 1988. For an airborne Doppler radar, where the Doppler velocity can be contaminated by platform motion and horizontal wind, the theoretical value of the uncertainty of the retrieved vertical air velocity as given in the previous section is less than $0.19\,\mathrm{m\,s^{-1}}$, at least for the studied cases, which makes this technique attractive even for the airborne radar. However, the retrieved vertical air velocity has never been compared with direct observations. Furthermore, a few assumptions are needed to estimate the total uncertainty in the previous section and it is unclear if these assumptions and the estimated theoretical uncertainty are reasonable. A comparison of the retrieved vertical
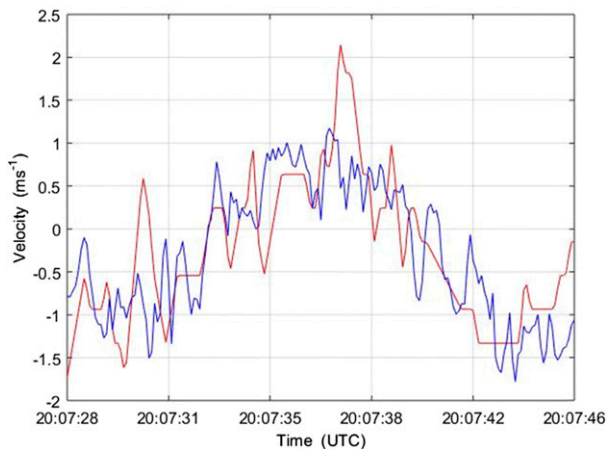
FIG. 12. Radar-retrieved (red; sampling 3 Hz) and in situ measured (blue; sampling 10 Hz) vertical air velocity for data observed in 22 May 2012 over Key West.

air velocity with those from in situ measurements will be used to evaluate the Mie retrieval technique. The 22 May 2012 case in Key West provides the results shown in Fig. 12 (time period between dashed lines in Fig. 8). The in situ measured velocity shown in Fig. 12 was obtained at a flight level about 500 m above the ground; the retrieved vertical air velocity was obtained at 15 m above the aircraft. Both in situ measurements and retrieved field show downdrafts before around 2007:32 UTC, updrafts between about 2007:32 and 2007:40 UTC, and downdrafts again after 2007:40 UTC. They agree well with each other and are highly coherent. To estimate uncertainties, first a linear interpolation is applied to the radar retrievals to transform the retrievals from 3 Hz to a 10-Hz dataset, and then a 9-point running average is applied to both the in situ measurements and radar retrievals to obtain trends. By subtracting the trend from each associated original data, one obtains the velocity residuals of the two datasets. The mean value of the trend and the standard deviation of the residual of the in situ measurements are -0.29 and $0.24\,\mathrm{m\,s^{-1}}$, respectively. Table 2 tabulates the difference between the radar-retrieved and in situ measured trends and the standard deviation of the velocity residual of the radar retrievals at heights from 15 to 105 m. At 15 m, the difference between two means of the trends is $0.01\,\mathrm{m\,s^{-1}}$, which indicates that the radar retrieval is almost equal to the in situ measurement. The standard deviation (STD) of the radar-retrieved velocity residual is $0.21\,\mathrm{m\,s^{-1}}$, which is a little bit lower than the STD of the in situ measured velocity residual. The lower value may reflect the fact that the turbulence with a scale smaller than beam size has been significantly attenuated because of beam filtering effect (Srivastava and Atlas 1974). Based upon the high consistency between retrievals and in situ measurements, it should be reasonable to deduce that the actual uncertainty of the radar retrieval is close to the in situ measurement uncertainty, which is about $0.1\,\mathrm{m\,s^{-1}}$ (Kalogiros and Wang 2002). This is lower than the theoretical value of $0.19\,\mathrm{m\,s^{-1}}$. The results in Table 2 demonstrate that, even at high levels, the radar retrievals and the in situ measurements are consistent and reflect a coherent layer in the vertical air velocity field. Calculations show that the correlation coefficient between radar and in situ measured trends has its highest value of 0.85 at 15 m above radar, and it is never smaller than 0.6 below 105 m.

Figure 13 shows a scatterplot of the radar retrievals and the in situ measurements at 15 m above radar. The black line is a reference line and has a slope of 1. The red line is obtained by means of an orthogonal regression analysis and its slope and intercept are 1.04 and 0.03, respectively. From another point of view, Fig. 13 demonstrates a very good agreement between radar retrievals and in situ measurements. The negligible intercept is an evidence of no systematic bias related to radar direct measurements and retrievals. The relatively high dispersion of the data might be attributed to the moderate turbulence in the cloud.

The above discussions justify the previous assumptions of beam pointing angle bias and uncertainty being small and insignificant. Given the high correlation between the results from two different methods shown in section 6, the discussions and results about the uncertainty of the Mie technique should apply to the results retrieved from the well-defined cloud droplets' peaks too. In this study, the sampling rate is 10 Hz for the in situ velocity measurements and 3 Hz for the radar observations, which is the reason for more high-frequency fluctuations in in situ measurements. This comparison is facilitated by the use of the FMCW radar (as compared with a pulsed radar), since it has no blind zone. Because noise dominates the data at

TABLE 2. Difference between mean trends of radar retrievals and in situ measurements and the standard deviation of radar retrievals at different heights.

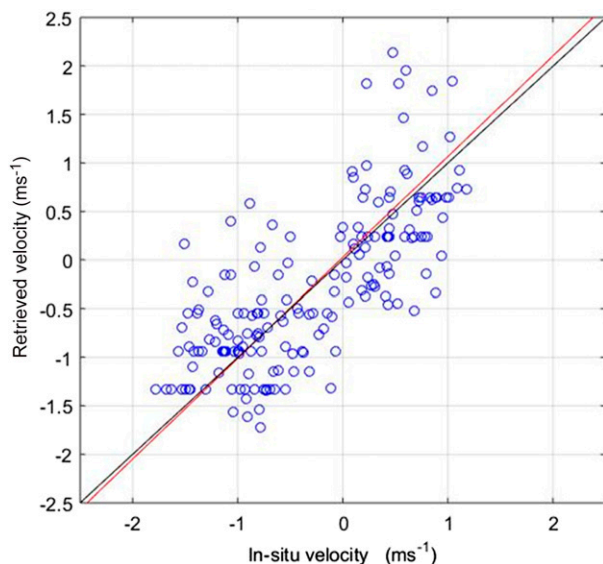| Height (m)	15	25	35	45	55	65	75	85	95	105
Difference of mean trends (m s^{-1})	0.01	-0.07	-0.07	-0.07	-0.07	-0.1	-0.05	-0.1	-0.09	-0.04
Std dev of radar retrievals (m s^{-1})	0.21	0.2	0.21	0.19	0.2	0.22	0.23	0.23	0.2	0.19

FIG. 13. Scatterplot of in situ measured vs radar-retrieved velocities at 15 m ARL obtained on 22 May 2012 over Key West.

the lowest two radar range gates, this comparison was not made for Barbados data.

8. Summary and conclusions

In this study, the potential of using an upward-pointing FMCW airborne cloud radar for the retrieval of vertical air motion is demonstrated for precipitating small cumuli observed during the BACEX and KWACEX field campaigns. It is the first demonstration of the Mie technique for vertical air velocity retrieval from an airborne cloud radar. In addition to the first Mie minimum, the first and second Mie maxima in radar Doppler spectra could be also used to retrieve vertical air velocity, but they are not as sharply defined as the first Mie minimum; this makes the first Mie minimum most suitable for this purpose. To retrieve the vertical air velocity aloft, the terminal speed of the Mie notch (i.e., 1.69-mm diameter droplet) needs to be corrected to compensate for the reduced air density. For the studied cases, this correction is about 0.2–$0.3\,\mathrm{m\,s^{-1}\,km^{-1}}$. For airborne radars, two major biases to the vertical air velocity retrieval result from the aircraft motion and the horizontal wind; the contribution due to the apparent rotational motion is negligible. These biases can be successfully removed by using the procedure described in this study. The deviation of the beam pointing angle from vertical can cause bias too. Calibration of the beam pointing angle is beyond the scope of this study, but the comparison with the in situ measurements shows that this bias, at least for the studied case, is small and negligible. In a bias-removed radar

Doppler spectrum, the vertical air velocity is the difference between the velocity of the Mie notch in still air and that in the bias-free spectrum. The vertical air velocity profile can be obtained from the Mie notch locations in the bias-free Doppler spectra at different heights. In addition to the Mie notch, a separate spectral peak due to the cloud droplets is simultaneously observed in the same radar Doppler spectra that contain the Mie signatures. The vertical air velocity retrieved using the Mie technique agrees well with that obtained directly from cloud droplets; the correlation coefficient is as high as 0.996. As a good tracer of vertical air motion, the spectral peak due to cloud droplets provides another possible method and opportunity to retrieve the vertical air velocity in clouds where the Mie notch is not applicable. However, this method requires users to make sure the spectral peak is due to cloud droplets. (Developing a universal method to recognize whether a power peak is a cloud droplet peak is beyond the scope of this study, but this identification can be easily done for the studied case by checking the relative locations of the Mie notch and the spectral peak on the right in Fig. 10.) Furthermore, the spectral peak due to cloud droplets might be broader and flatter and not as well defined as Mie notch, which can cause larger uncertainty in retrieved vertical air velocity.

In addition to removable bias, the vertical velocity retrieval suffers from various uncertainties such as aircraft attitude angle and velocity, beam pointing angle, Mie notch positioning, velocity quantization, and Doppler fading. The total theoretical uncertainty for the studied cases is less than $0.19\,\mathrm{m\,s^{-1}}$, which makes the Mie notch vertical velocity retrieval technology attractive even for the airborne radar. However, it is noteworthy that Doppler fading can broaden spectrum width and reduce the Mie notch detectability as well as increase the uncertainty. To keep the related uncertainty under $0.1\,\mathrm{m\,s^{-1}}$ for an aircraft moving at $200\,\mathrm{m\,s^{-1}}$, a radar with beamwidth narrower than $0.21°$ must be used to ensure spectral broadening due to Doppler fading is below $0.22\,\mathrm{m\,s^{-1}}$.

The retrieved vertical air velocity time–height field clearly shows that the vertical air velocity structures and features are different from those in mean Doppler velocity field and those in bias-free field, and should be more directly related to the cloud dynamics and microphysics. The unique dataset shown here demonstrates that the vertical air velocity retrieved from the Mie technique at 15 m above radar is highly coherent and agrees well with the in situ measurements obtained near the cloud base but in the cloud. At the lowest available radar range gate, the difference between the mean trends of the radar-retrieved velocity and in situ measurement is $0.01\,\mathrm{m\,s^{-1}}$, which again indicates a good agreement between the radar retrieval and the in situ

measurement. The standard deviation of the residuals of the radar retrievals is $0.21\,\mathrm{m\,s^{-1}}$, which is a little bit less than the STD of the in situ measured velocity because of the beam filtering effect. The uncertainty of the radar retrievals is about $0.1\,\mathrm{m\,s^{-1}}$, and lower than the theoretical value $0.19\,\mathrm{m\,s^{-1}}$. The conclusions about the uncertainties of Mie technique are also valid and applicable to retrievals from cloud spectral peaks as long as the peaks are well defined.

These results demonstrate that the first Mie minimum, combined with the procedures of platform motion and horizontal wind removal described in this study, can be successfully applied to airborne cloud Doppler radar data to retrieve 2D vertical air motion fields in clouds. Possible applications of this technique include the mapping of vertical air velocity fields in hurricanes and tropical storm rainbands and in warm cloud systems that have precipitation drops greater than 1.69 mm. Although the Mie notch may not always exist or be detectable, considering the vertical velocity, especially the vertical velocity profile in clouds and storms that is not easy to obtain, the method described herein has valuable potential.

APPENDIX A

Formulas for Removal of Contamination Motions

L1994 employed an angle between the radar beam and X–O–Z plane; for example, τ in their Fig. 3 that allows a convenient determination of a sampling volume location and the direction of position vector for their scanning beam. For our case, in an aircraft-relative coordinate system, the radar beam is fixed and located in plane Y–O–Z. Thus, angle τ is not needed and the azimuth is equal to $0°$ or $\lambda = 0$ (refer to Fig. 3 of L1994). The aircraft-relative Cartesian components of a position vector, x_a, y_a, and z_a, or Eq. (4) of L1994 can be rewritten as

$$\begin{pmatrix} x_a \\ y_a \\ z_z \end{pmatrix} = r \begin{pmatrix} 0 \\ \cos\phi \\ \sin\phi \end{pmatrix}, \tag{A1}$$

where r is the slant range from radar to an investigated radar resolution volume and φ is the elevation angle. In an Earth-relative coordinate system, the Cartesian components of the vector are

$$\begin{pmatrix} x \\ y \\ z \end{pmatrix} = \mathbf{M}_T \mathbf{M}_D \mathbf{M}_P \mathbf{M}_R \begin{pmatrix} x_a \\ y_a \\ z_a \end{pmatrix}, \tag{A2}$$

where $\mathbf{M}_T$, $\mathbf{M}_D$, $\mathbf{M}_P$, and $\mathbf{M}_R$ are transformation matrices given by L1994. Substituting the expressions of $\mathbf{M}_T$, $\mathbf{M}_D$, $\mathbf{M}_P$, and $\mathbf{M}_R$ into the above equation, one has

$$\begin{pmatrix} x \\ y \\ z \end{pmatrix} = r \begin{pmatrix} \cos H \sin R \sin\phi + \sin H \cos P \cos\phi - \sin H \sin P \cos R \sin\phi \\ \cos H \cos P \cos\phi - \sin H \sin R \sin\phi - \cos H \sin P \cos R \sin\phi \\ \sin P \cos\phi + \cos P \cos R \sin\phi \end{pmatrix}, \tag{A3}$$

where H is the heading of the aircraft, R is the roll angle, and P is the pitch angle. Using Eq. (4) and Eq. (19) of L1994 and going through a series of mathematical manipulations similar to those given by L1994, one can obtain an analytical expression for a radar-measured Doppler velocity that is similar to the Eq. (26) of L1994. However, we are not interested in the Doppler velocity here. What we are interested in is the vertical air velocity. With a little further mathematical manipulation, one can easily obtain the analytical expressions of Eqs. (3) that are rewritten here for completeness as

$$w - v_t = \frac{V_m - I_1 + I_2 - I_3 - I_4}{\sin\phi} + W_a, \tag{A4a}$$

$$I_1 = \frac{ux + vy}{r}, \tag{A4b}$$

$$I_2 = \frac{V_a(x\sin T + y\cos T)}{r}, \tag{A4c}$$

$$I_3 = -\frac{Lx}{r}\left[(1 + \cos P)\cos H\frac{dH}{dt} - \sin P\sin H\frac{dP}{dt}\right], \tag{A4d}$$

and

$$I_4 = -\frac{L}{r}\left\{z\cos P\frac{dP}{dt} - y\left[(1 + \cos P)\sin H\frac{dH}{dt} + \sin P\cos H\frac{dP}{dt}\right]\right\}, \tag{A4e}$$
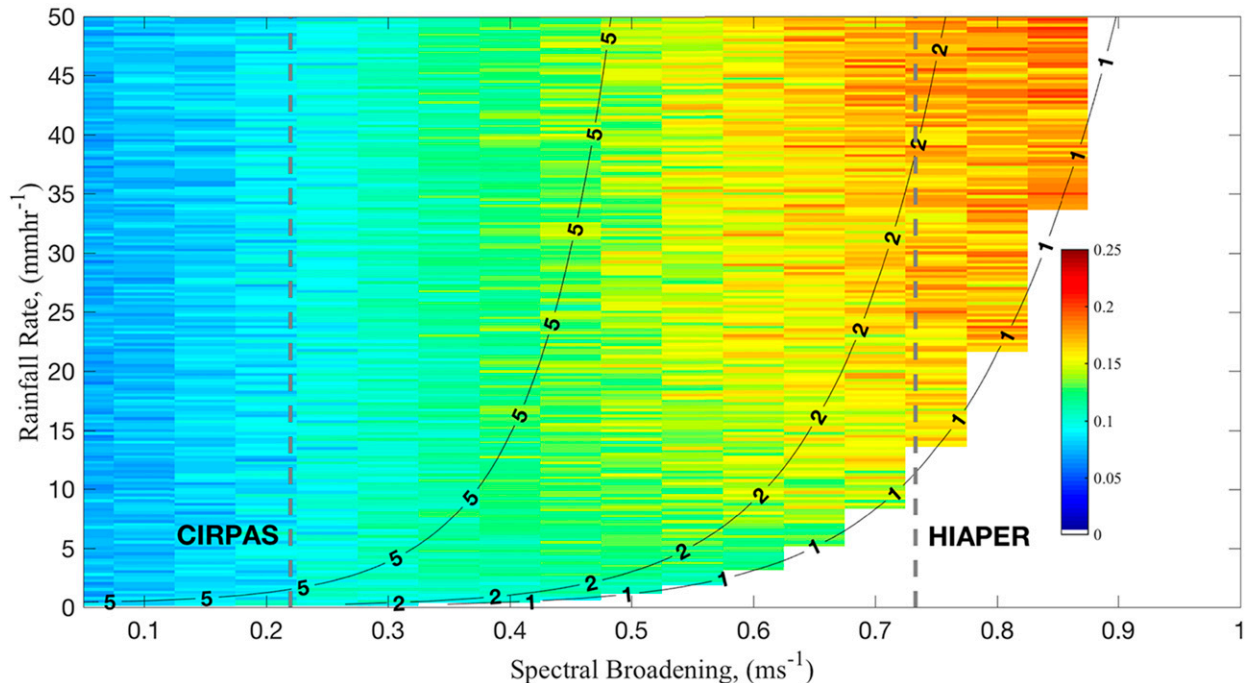
FIG. B1. Different colors show the velocity standard deviation of Mie minima uncertainty (m s^{-1}). The dashed vertical line indicates the spectrum broadening due to Doppler fading for the TO (used in this study) and HIAPER aircraft, respectively. The black contours show the spectral density difference between the first Mie maximum and first Mie minimum.

where V_m is the radar-measured radial velocity, W_a is the vertical velocity of the aircraft relative to the ground, u is the component of horizontal wind in the east direction, v is the component of horizontal wind in the north direction, V_a is the horizontal velocity of the aircraft relative to the ground, T is the sum of the heading and drift angle, and L is the distance between radar antenna and GPS navigation unit. By using Eq. (A4) or Eq. (3), the aircraft motion and impact from horizontal wind, as well as apparent motion due to the radar antenna being located some distance away from the navigation unit, can be removed.

APPENDIX B

Impact of Doppler fading on the Detection of the Mie Minima

Our ability to detect the Mie minimum in the 94-GHz airborne radar Doppler spectra depends on two factors: the shape of the raindrop size distribution and the spectral broadening introduced by the platform motion. Assuming an exponential raindrop size distribution, the slope of the particle size distribution Λ (mm^{-1}) is related to the rainfall rate R (mm h^{-1}) through the relationship $\Lambda = 4.1R^{-0.21}$ (Marshall and Palmer 1948). The slope Λ determines the number concentration ratio of the

raindrops that contribute to the first and second Mie maxima and subsequently determines their relative strength in the observed radar Doppler spectra (Kollias et al. 2002). The higher the second spectral peak (lower Λ or higher R) the deeper the Mie scattering valley (minimum) and the higher the probability that we will detect the Mie minimum. The second factor that controls our ability to detect the Mie minimum is the spectral broadening σ_D (m s^{-1}) due to turbulence and platform motion. The parameter σ_D determines the width of a Gaussian function that will convoluted with the quiet (no air motion) raindrop radar Doppler spectra. The higher the σ_D, the higher the degree of smearing of the Mie resonant signatures in the radar Doppler spectra, and subsequently the lower the probability of detecting the Mie minimum.

Here, numerical simulations of 94-GHz radar Doppler spectra for a wide range of rainfall rates and spectral broadening were carried out. The Nyquist velocity of the simulated radar Doppler spectra is 8 m s^{-1} (corresponding to a pulse repetition frequency of 10 kHz), the number of FFT points is 512, with 10 spectral averages and assuming receiver noise of -30 dBZ. For each pair of R and σ_D conditions, 100 synthetic radar Doppler spectra were generated, and the Mie minimum was detected using a local search for the minimum simulated spectral density. Using the 100 samples, the standard

deviation of the velocity where the Mie minimum was detected and estimated. Figure B1 shows the standard deviation for a wide range of R and σ_D values. At low spectra broadening conditions, the standard deviation is below $0.1 \, \mathrm{m \, s^{-1}}$; however, values higher than $0.2 \, \mathrm{m \, s^{-1}}$ are observed at higher spectral broadening conditions. The difference in dB between the spectral density of the second Mie peak and the first Mie minimum is shown by the contours. As expected, the deeper the Mie minimum depression, the lower the uncertainty in the estimation of the Mie minimum location. We can see that for spectral broadening values of $0.9 \, \mathrm{m \, s^{-1}}$ or higher, we cannot detect the Mie minimum independent of the rainfall rate or slope. For an aircraft with speed V_A ($\mathrm{m \, s^{-1}}$), the spectral broadening σ_D ($\mathrm{m \, s^{-1}}$) given by $\sigma_D \approx 0.3 V_A \theta_{3\mathrm{dB}}$ where $\theta_{3\mathrm{dB}}$ is the 3-dB beamwidth of the antenna in radians (Sloss and Atlas 1968; Kollias et al. 2014; Kobayashi 2002; Kobayashi et al. 2002). The CIRPAS Twin Otter 94-GHz FMCW system has a 0.7° beamwidth and an airspeed of $60 \, \mathrm{m \, s^{-1}}$. For comparison, the NCAR/NSF High-Performance Instrumented Airborne Platform for Environmental Research (HIAPER) 94-GHz radar has a beamwidth of 0.68° and an airspeed of $200 \, \mathrm{m \, s^{-1}}$. Under these conditions, the average spectral broadening introduced by the aircraft motion is 0.22 and $0.73 \, \mathrm{m \, s^{-1}}$ for the TO and NCAR aircraft, respectively (Fig. B1, vertical lines). For the aforementioned analysis, it is clear that the slow moving Twin Otter results in relatively small spectral broadening, thus enabling the detection of the Mie minima for all rainfall rate conditions. On the other hand, the fast-moving HIAPER aircraft introduces much higher spectral broadening, thus making the detection of the Mie minima challenging, especially for low rainfall rates.

REFERENCES

Beard, K. V., 1985: Simple altitude adjustments to raindrop velocities for Doppler radar analysis. *J. Atmos. Oceanic Technol.*, **2**, 468–471, doi:10.1175/1520-0426(1985)002<0468:SAATRV>2.0.CO;2.

Doviak, R. J., and D. S. Zrnić, 1993: *Doppler Radar and Weather Observations.* 2nd ed. Academic Press, 562 pp.

Fang, M., and R. J. Doviak, 2008: Coupled contributions in the Doppler radar spectrum width equation. *J. Atmos. Oceanic Technol.*, **25**, 2245–2258, doi:10.1175/2007JTECHA968.1.

——, ——, and B. A. Albrecht, 2012: Analytical expressions for Doppler spectra of scatter from hydrometeors observed with a vertically directed radar beam. *J. Atmos. Oceanic Technol.*, **29**, 500–509, doi:10.1175/JTECH-D-11-00005.1.

French, J. R., G. Vali, and R. D. Kelly, 1999: Evolution of small cumulus clouds in Florida: Observations of pulsating growth. *Atmos. Res.*, **52**, 143–165, doi:10.1016/S0169-8095(99)00024-1.

Giangrande, S. E., E. P. Luke, and P. Kollias, 2010: Automated retrievals of precipitation parameters using non-Rayleigh scattering at 95 GHz. *J. Atmos. Oceanic Technol.*, **27**, 1490–1503, doi:10.1175/2010JTECHA1343.1.

Gossard, E. E., 1988: Measuring drop-size distributions in clouds with a clear-air-sensing Doppler radar. *J. Atmos. Oceanic Technol.*, **5**, 640–649, doi:10.1175/1520-0426(1988)005<0640:MDSDIC>2.0.CO;2.

Guimond, S. R., G. M. Heymsfield, and F. J. Turk, 2010: Multiscale observations of Hurricane Dennis (2005): The effects of hot towers on rapid intensification. *J. Atmos. Sci.*, **67**, 633–654, doi:10.1175/2009JAS3119.1.

Gunn, R., and G. D. Kinzer, 1949: The terminal velocity of fall for water droplets in stagnant air. *J. Meteor.*, **6**, 243–248, doi:10.1175/1520-0469(1949)006<0243:TTVOFF>2.0.CO;2.

Haimov, S., and A. Rodi, 2013: Fixed-antenna pointing-angle calibration of airborne Doppler cloud radar. *J. Atmos. Oceanic Technol.*, **30**, 2320–2335, doi:10.1175/JTECH-D-12-00262.1.

Heymsfield, G. M., 1989: Accuracy of vertical air motions from nadir-viewing Doppler airborne radars. *J. Atmos. Oceanic Technol.*, **6**, 1079–1082, doi:10.1175/1520-0426(1989)006<1079:AOVAMF>2.0.CO;2.

——, and Coauthors, 1996: The EDOP radar system on the high-altitude NASA ER-2 aircraft. *J. Atmos. Oceanic Technol.*, **13**, 795–809, doi:10.1175/1520-0426(1996)013<0795:TERSOT>2.0.CO;2.

Jung, E., B. A. Albrecht, G. Feingold, H. H. Jonsson, P. Chuang, and S. L. Donaher, 2016a: Aerosols, clouds, and precipitation in the North Atlantic trades observed during the Barbados Aerosol Cloud Experiment. Part I: Distributions and variability. *Atmos. Chem. Phys.*, **16**, 8643–8666, doi:10.5194/acp-16-8643-2016.

——, ——, A. Sorooshian, P. Zuidema, and H. H. Jonsson, 2016b: Precipitation susceptibility in marine stratocumulus and shallow cumulus from airborne measurements. *Atmos. Chem. Phys.*, **16**, 11 395–11 413, doi:10.5194/acp-16-11395-2016.

Kalogiros, J. A., and Q. Wang, 2002: Calibration of a radome-differential GPS system on a Twin Otter research aircraft for turbulence measurements. *J. Atmos. Oceanic Technol.*, **19**, 159–171, doi:10.1175/1520-0426(2002)019<0159:COARDG>2.0.CO;2.

Kobayashi, S., 2002: A unified formalism of incoherent, quasi-coherent, and coherent correlation signals on pulse-pair Doppler operation for a cloud-profiling radar: Aiming for a space mission. *J. Atmos. Oceanic Technol.*, **19**, 443–456, doi:10.1175/1520-0426(2002)019<0443:AUFOIQ>2.0.CO;2.

——, H. Kumagai, and H. Kuroiwa, 2002: A proposal of pulse-pair Doppler operation on a spaceborne cloud-profiling radar in the W band. *J. Atmos. Oceanic Technol.*, **19**, 1294–1306, doi:10.1175/1520-0426(2002)019<1294:APOPPD>2.0.CO;2.

Kollias, P., B. A. Albrecht, R. Lhermitte, and A. Savtchenko, 2001: Radar observations of updrafts, downdrafts, and turbulence in fair-weather cumuli. *J. Atmos. Sci.*, **58**, 1750–1766, doi:10.1175/1520-0469(2001)058<1750:ROOUDA>2.0.CO;2.

——, ——, and F. Marks Jr., 2002: Why Mie? Accurate observations of vertical air velocities and raindrops using a cloud radar. *Bull. Amer. Meteor. Soc.*, **83**, 1471–1483, doi:10.1175/BAMS-83-10-1471.

——, ——, and ——, 2003: Cloud radar observations of vertical drafts and microphysics in convective rain. *J. Geophys. Res.*, **108**, 4053, doi:10.1029/2001JD002033.

——, E. E. Clothiaux, M. A. Miller, B. A. Albrecht, G. L. Stephens, and T. P. Ackerman, 2007: Millimeter-wavelength radars: New frontier in atmospheric cloud and precipitation research. *Bull. Amer. Meteor. Soc.*, **88**, 1608–1624, doi:10.1175/BAMS-88-10-1608.

——, S. Tanelli, A. Battaglia, and A. Tatarevic, 2014: Evaluation of EarthCARE cloud profiling radar Doppler velocity measurements

in particle sedimentation regimes. *J. Atmos. Oceanic Technol.*, **31**, 366–386, doi:10.1175/JTECH-D-11-00202.1.

Lee, W.-C., P. Dodge, F. Marks, and P. Hildebrand, 1994: Mapping of airborne Doppler radar data. *J. Atmos. Oceanic Technol.*, **11**, 572–578, doi:10.1175/1520-0426(1994)011<0572:MOADRD>2.0.CO;2.

Lhermitte, R., 1988: Observation of rain at vertical incidence with a 94 GHz Doppler radar: An insight of Mie scattering. *Geophys. Res. Lett.*, **15**, 1125–1128, doi:10.1029/GL015i010p01125.

——, 2002: *Centimeter and Millimeter Wavelength Radars in Meteorology.* A&A Printing, 550 pp.

Li, L., G. M. Heymsfield, P. E. Racette, L. Tian, and E. Zenker, 2004: A 94-GHz cloud radar system on a NASA high-altitude ER-2 aircraft. *J. Atmos. Oceanic Technol.*, **21**, 1378–1388, doi:10.1175/1520-0426(2004)021<1378:AGCRSO>2.0.CO;2.

Lorsolo, S., J. Zhang, F. D. Marks, and J. Gamache, 2010: Estimation and mapping of hurricane turbulent energy using airborne Doppler measurements. *Mon. Wea. Rev.*, **138**, 3656–3670, doi:10.1175/2010MWR3183.1.

Marshall, J. S., and W. Palmer, 1948: The distribution of raindrops with size. *J. Meteor.*, **5**, 165–166, doi:10.1175/1520-0469(1948)005<0165:TDORWS>2.0.CO;2.

Mätzler, C., 2002: Matlab function for Mie scattering and absorption. Universitas Bernensis Institut für Angewandte Physik Research Rep. 2002-11, 24 pp.

May, P. T., and D. K. Rajopadhyaya, 1996: Wind profiler observations of vertical motion and precipitation microphysics of a tropical squall line. *Mon. Wea. Rev.*, **124**, 621–633, doi:10.1175/1520-0493(1996)124<0621:WPOOVM>2.0.CO;2.

Mead, J. B., I. PopStefanija, P. Kollias, B. A. Albrecht, and R. Bluth, 2003: Compact airborne solid-state 95 GHz FMCW radar system. *31st Int. Conf. on Radar Meteorology*, Seattle, WA, Amer. Meteor. Soc., 4A.3. [Available online at https://ams.confex.com/ams/pdfpapers/63494.pdf.]

Mie, G., 1908: Beitrage Optik trüber Medien, speziell kolloidaler Metallösungen (Contributions to the optics of diffuse media, especially colloid metal solutions). *Ann. Phys.*, **330**, 377–445, doi:10.1002/andp.19083300302.

Mishchenko, M. I., L. D. Travis, and D. W. Mackowski, 1996: T-matrix computations of light scattering by nonspherical particles: A review. *J. Quant. Spectrosc. Radiat. Transfer*, **55**, 535–575, doi:10.1016/0022-4073(96)00002-7.

Nielsen, J. W., 1992: In situ observations of Kelvin–Helmholtz waves along a frontal inversion. *J. Atmos. Sci.*, **49**, 369–386, doi:10.1175/1520-0469(1992)049<0369:ISOOKH>2.0.CO;2.

Noh, Y. J., C. J. Seaman, T. H. Vonder Haar, and G. Liu, 2013: In situ aircraft measurements of the vertical distribution of liquid and ice water content in midlatitude mixed-phase clouds. *J. Appl. Meteor. Climatol.*, **52**, 269–279, doi:10.1175/JAMC-D-11-0202.1.

Papoulis, A., and S. U. Pallai, 2004: *Probability, Random Variables, and Stochastic Processes.* McGraw Hill, 852 pp.

Probert-Jones, J. R., and W. G. Harper, 1961: Vertical air motion in showers as revealed by Doppler radar. *Proc. Ninth Weather Radar Conf.*, Kansas City, MO, Amer. Meteor. Soc., 225–232.

Rajopadhyaya, D. K., P. T. May, R. Cifelli, S. K. Avery, C. R. Williams, W. L. Ecklund, and K. S. Gage, 1998: The effect of vertical air motions on rain rates and median volume diameter determined from combined UHF and VHF wind profiler measurements and comparisons with rain gauge measurements. *J. Atmos. Oceanic Technol.*, **15**, 1306–1319, doi:10.1175/1520-0426(1998)015<1306:TEOVAM>2.0.CO;2.

Rogers, R. R., D. Baumgardner, S. A. Ethier, D. A. Carter, and W. L. Ecklund, 1993: Comparison of raindrop size distributions measured by radar wind profiler and by airplane. *J. Appl. Meteor.*, **32**, 694–699, doi:10.1175/1520-0450(1993)032<0694:CORSDM>2.0.CO;2.

Rogers, R., P. Reasor, and S. Lorsolo, 2013: Airborne Doppler observations of the inner-core structural differences between intensifying and steady-state tropical cyclones. *Mon. Wea. Rev.*, **141**, 2970–2991, doi:10.1175/MWR-D-12-00357.1.

Savitzky, A., and M. J. E. Golay, 1964: Smoothing and differentiation of data by simplified least squares procedures. *Anal. Chem.*, **36**, 1627–1639, doi:10.1021/ac60214a047.

Schafer, R. W., 2011: What is a Savitzky–Golay filter? *IEEE Signal Process. Mag.*, **28**, 111–117, doi:10.1109/MSP.2011.941097.

Sloss, P. W., and D. Atlas, 1968: Wind shear and reflectivity gradient effect on Doppler spectra. *J. Atmos. Sci.*, **25**, 1080–1089, doi:10.1175/1520-0469(1968)025<1080:WSARGE>2.0.CO;2.

Srivastava, R. C., and D. Atlas, 1974: Effect of finite radar pulse volume on turbulence measurements. *J. Appl. Meteor.*, **13**, 472–480, doi:10.1175/1520-0450(1974)013<0472:EOFRPV>2.0.CO;2.

Stith, J. L., 1995: In situ measurements and observations of cumulonimbus mamma. *Mon. Wea. Rev.*, **123**, 907–914, doi:10.1175/1520-0493(1995)123<0907:ISMAOO>2.0.CO;2.

Sy, O. O., S. Tanelli, N. Takahashi, Y. Ohno, H. Horie, and P. Kollias, 2014: Simulation of EarthCARE spaceborne Doppler radar products using ground-based and airborne data: Effects of aliasing and nonuniform beam-filling. *IEEE Trans. Geosci. Remote Sens.*, **52**, 1463–1479, doi:10.1109/TGRS.2013.2251639.

Tanelli, S, E. Im, S. L. Durden, L. Facheris, and D. Giuli, 2002: The effects of nonuniform beam filling on vertical rainfall velocity measurements with a spaceborne Doppler radar. *J. Atmos. Oceanic Technol.*, **19**, 1019–1034, doi:10.1175/1520-0426(2002)019<1019:TEONBF>2.0.CO;2.

Tridon, F., and A. Battaglia, 2015: Dual-frequency radar Doppler spectral retrieval of rain drop size distributions and entangled dynamics variables. *J. Geophys. Res. Atmos.*, **120**, 5585–5601, doi:10.1002/2014JD023023.

——, ——, and P. Kollias, 2013: Disentangling Mie and attenuation effects in rain using a K_a-W dual-wavelength Doppler spectral ratio technique. *Geophys. Res. Lett.*, **40**, 5548–5552, doi:10.1002/2013GL057454.

Wakasugi, K., A. Mizutani, M. Matsuo, S. Fukao, and S. Kato, 1986: A direct method for deriving drop-size distribution and vertical air velocities from VHF Doppler radar spectra. *J. Atmos. Oceanic Technol.*, **3**, 623–629, doi:10.1175/1520-0426(1986)003<0623:ADMFDD>2.0.CO;2.

Wang, Z., and Coauthors, 2012: Single aircraft integration of remote sensing and in-situ sampling for the study of cloud microphysics and dynamics. *Bull. Amer. Meteor. Soc.*, **93**, 653–668, doi:10.1175/BAMS-D-11-00044.1.